

See discussions, stats, and author profiles for this publication at: <https://www.researchgate.net/publication/283829744>

# Self-Assembly of ABC Triblock Copolymer under 3D Soft Confinement: A Monte Carlo Study

ARTICLE *in* SOFT MATTER · NOVEMBER 2015

Impact Factor: 4.03 · DOI: 10.1039/C5SM02079D

---

READS

12

3 AUTHORS, INCLUDING:



Yutian Zhu

Chinese Academy of Sciences

43 PUBLICATIONS 355 CITATIONS

SEE PROFILE



Cite this: DOI: 10.1039/c5sm02079d

# Self-assembly of ABC triblock copolymers under 3D soft confinement: a Monte Carlo study

Nan Yan,<sup>ab</sup> Yutian Zhu<sup>\*a</sup> and Wei Jiang<sup>a</sup>

Under three-dimensional (3D) soft confinement, block copolymers can self-assemble into unique nanostructures that cannot be fabricated in an un-confined space. Linear ABC triblock copolymers containing three chemically distinct polymer blocks possess relatively complex chain architecture, which can be a promising candidate for the 3D confined self-assembly. In the current study, the Monte Carlo technique was applied in a lattice model to study the self-assembly of ABC triblock copolymers under 3D soft confinement, which corresponds to the self-assembly of block copolymers confined in emulsion droplets. We demonstrated how to create various nanostructures by tuning the symmetry of ABC triblock copolymers, the incompatibilities between different block types, and solvent properties. Besides common pupa-like and bud-like nanostructures, our simulations predicted various unique self-assembled nanostructures, including a striped-pattern nanoparticle with intertwined A-cages and C-cages, a pyramid-like nanoparticle with four Janus B–C lamellae adhered onto its four surfaces, an ellipsoidal nanoparticle with a dumbbell-like A-core and two Janus B–C lamellae and a Janus B–C ring surrounding the A-core, a spherical nanoparticle with a A-core and a helical Janus B–C stripe around the A-core, a cubic nanoparticle with a cube-shape A-core and six Janus B–C lamellae adhered onto the surfaces of the A-cube, and a spherical nanoparticle with helical A, B and C structures, from the 3D confined self-assembly of ABC triblock copolymers. Moreover, the formation mechanisms of some typical nanostructures were also examined by the variations of the contact numbers with time and a series of snapshots at different Monte Carlo times. It is found that ABC triblock copolymers usually aggregate into a loose aggregate at first, and then the microphase separation between A, B and C blocks occurs, resulting in the formation of various nanostructures.

Received 19th August 2015,  
Accepted 4th November 2015

DOI: 10.1039/c5sm02079d

www.rsc.org/softmatter

## Introduction

Recently, the self-assembly of block copolymers (BCPs) under 3D confinement has attracted increasing attention since the confinement effect can effectively break the symmetry of a structure, resulting in some new nanostructures that cannot be obtained by other methods.<sup>1–8</sup> Up to now, great efforts have been made to fabricate block copolymer nanoparticles with abundant internal microphase-separated nanostructures due to their potential applications as catalyst carriers, dielectric resonators, drug delivery systems, and photonic crystals.<sup>9,10</sup> Basically, the confinements can be divided into two categories, hard confinement and soft confinement.<sup>7</sup> If the confining boundary is the hard surface, the shape of the confining geometry is always fixed. This kind of confinement is termed hard confinement. In contrast to hard

confinement, soft confinement refers to the confinement when the confining geometry is not fixed but deformable, such as the cells or emulsion droplets.

When confined within a spherical space, BCPs can spontaneously self-assemble into a variety of unique nanostructures, depending on various control parameters, including the size of the confined space, the intrinsic properties of BCPs, polymer–surface interactions, and so forth.<sup>1,11–19</sup> For instance, Liang and coworkers investigated the self-assembly of AB diblock copolymers confined in a solid spherical space *via* the Monte Carlo method.<sup>1</sup> It was found that the symmetric diblock copolymers are more likely to form the onion-like multilayer structure. Yu *et al.* predicted a large number of interesting patchy nanoparticles self-assembled from linear triblock copolymers under solid spherical confinement.<sup>19</sup> Compared to the self-assembly under solid confinement, the self-assembly of block copolymers confined in the emulsion droplet, *i.e.* under 3D soft confinement, has received more and more attention these years. For example, Zhu and coworkers fabricated mesoporous BCP nanoparticles with tailored pore structures, taking advantage of supramolecular chemistry and 3D confined assembly of block copolymers.<sup>14</sup> Yang and Zhu generated nanostructured particles

<sup>a</sup> State Key Laboratory of Polymer Physics and Chemistry,  
Changchun Institute of Applied Chemistry, Chinese Academy of Sciences,  
Changchun 130022, People's Republic of China. E-mail: ytzhu@ciac.ac.cn;  
Fax: +86-43185262126; Tel: +86-43185262866

<sup>b</sup> University of Chinese Academy of Sciences, Beijing 100049,  
People's Republic of China

via the self-assembly of polystyrene-*b*-poly(4-vinylpyridine) (penta-decylphenol) (PS-*b*-P4VP (PDP)) under 3D soft confinement.<sup>15</sup> The internal structures of the resulting nanoparticles can be readily tuned by varying the PDP content. Yi and Yang obtained various unprecedented structural motifs by cooperative self-assembly of block copolymers and amphiphilic block copolymer surfactants within emulsion droplets.<sup>13</sup> Besides experimental studies, Li and coworkers recently proposed a simulated annealing method to mimic the self-assembly of diblock copolymers confined in the emulsion droplets.<sup>7</sup> The soft confinement was achieved by the formation of polymer droplets in a poor solvent environment, which corresponded well with the self-assembly of block copolymers confined in emulsion droplets.

On the other hand, it has been reported that linear ABC triblock copolymers, comprising of three chemically distinct polymer blocks covalently linked together, are versatile precursors for the fabrication of various interesting multicompartment micelles, such as helices, raspberry-like particles, hamburger-like particles, Janus particles, segmented cylinders, and segmented wormlike micelles.<sup>20–32</sup> For example, Zhu *et al.* fabricated the giant segmented wormlike micelles from the self-assembly of linear poly(styrene-*b*-2-vinylpyridine-*b*-ethylene oxide) triblock copolymers in a dilute solution.<sup>16</sup> Liu and coworkers reported the unique double helices from the self-assembly of the poly(*n*-butyl methacrylate)-*b*-poly(2-cinnamoyloxyethyl methacrylate)-*b*-poly(*tert*-butyl acrylate) (PBMA-*b*-PCEMA-*b*-PtBA) triblock copolymer.<sup>24</sup> However, self-assembly of ABC triblock copolymers under 3D soft confinement was seldom investigated either in experiments or in computer simulations. Very recently, Zhu and coworkers examined the self-assembly of polystyrene-*b*-polyisoprene-*b*-poly(2-vinylpyridine) confined in emulsion droplets.<sup>17</sup> They observed that the morphologies of the self-assembled nanoparticles can be tuned from onion-like to bud-like, pupa-like, and then back to pupa-like and onion-like particles by tailoring the properties of the surfactants. Because of the complex chain architecture of ABC triblock copolymer and the relatively complicated interactions among the three blocks and the interface, a clear understanding of the self-assembly of ABC triblock copolymers under the 3D soft confinement is far away.

In the current study, we applied Monte Carlo simulations to systematically investigate the self-assembly of linear ABC triblock copolymers under 3D soft confinement. The simulations predicted a rich variety of unique nanostructures from the self-assembly of ABC triblock copolymers under 3D soft confinement. Moreover, the formation mechanisms for some typical nanoparticles were also examined.

## Model and method

The Monte Carlo method was performed in this work to mimic the self-assembly of linear ABC triblock copolymers under 3D soft confinement. All the simulations were carried out in a  $50 \times 50 \times 50$  simple cubic lattice by the self-avoiding chain model. Periodic boundary conditions were imposed in all three directions. The single-site bond fluctuation model restricting the bond length to either 1 or  $\sqrt{2}$  was used.<sup>33–35</sup> Excluded volume interactions were always enforced to ensure that not more than one

monomer occupied the same lattice site and no bond crossing was allowed. This means that each lattice site is occupied by either a polymer bead or a vacancy (a solvent). Evolution of the polymer chain was achieved through the exchange move between the polymer bead and the vacancy. A polymer bead was chosen randomly to make an attempted exchange with one of its 18 nearest-neighbor sites. To enhance the simulation efficiency, the partial-reptation algorithm was applied only if the selected polymer bead cannot make an exchange with any of the 18 nearest-neighbor sites because of the violation of excluded volume conditions or the no bond-crossing or the bond length restrictions.<sup>36,37</sup> The acceptance or rejection of the attempted exchange was further determined by the Metropolis rule.<sup>38</sup> This rule states that the attempted exchange is accepted if the energy change  $\Delta E$  is negative. Otherwise, the exchange will be accepted with a probability of  $p = \exp[-\Delta E/k_B T]$ , where  $\Delta E = \sum_{ij} \Delta N_{ij} \epsilon_{ij}$  is the energy change in one attempted exchange;  $k_B$  is the Boltzmann constant and set as 1;  $T$  is the reduced temperature,  $\Delta N_{ij}$  is the number difference between the nearest neighbor pairs of components *i* and *j* before and after the exchange,  $\epsilon_{ij}$  is the reduced interaction between components *i* and *j*; *i, j* = A, B, C and S (solvent), respectively.

In experiments of the emulsion-evaporation induced self-assembly, BCPs were dissolved in organic solvent (good solvent) at first, and then were emulsified in water (poor solvent). As the organic solvent was evaporated, BCPs tended to aggregate into a polymer droplet, which was surrounded by the water. On the other hand, the microphase separation between the different block types occurred simultaneously, resulting in a large number of well-defined nanostructures. In the previous studies, the annealing method was proposed to mimic the emulsion-evaporation induced self-assembly in experiments.<sup>7,18</sup> In simulations, the inverse temperature  $1/T$  changed gradually from 0 (an athermal state of  $T = \infty$ ) to 0.07, which represents the system changing from an athermal state to a relatively low temperature state. The annealing rate was kept at 0.0002 per step in this study. This annealing process caused BCPs to gradually aggregate into the polymer droplets when a solvent environment is changed from a good solvent to a poor solvent, corresponding well to emulsion-evaporation induced self-assembly of polymers in experiments. The annealing process was completed in 350 steps at an annealing rate of 0.0002 per step. After the annealing process,  $1/T$  was kept as 0.07, and another 650 annealing steps were carried out to ensure that the final structures were in an equilibrium state. In each annealing step, 9000 Monte Carlo steps (MCSs) were performed. One MCS means that each bead has one attempted exchange move on average.

In all the simulations, the concentration of the block copolymers was fixed at 10% (*i.e.* 595 polymer chains in the system) and the chain length was set as  $L_c = 21$ , *i.e.*  $L_A + L_B + L_C = 21$ . All other self-interactions between the same components, *i.e.*  $\epsilon_{AA}$ ,  $\epsilon_{BB}$ ,  $\epsilon_{CC}$ , and  $\epsilon_{SS}$  were set as 0. The polymer–polymer interactions between the different polymer components were set as  $\epsilon_{AB} = \epsilon_{AC} = \epsilon_{BC} = 3.0$  to mimic the incompatibilities between different block types. The polymer–solvent interactions,  $\epsilon_{AS}$ ,  $\epsilon_{BS}$  and  $\epsilon_{CS}$ , were set to positive values to ensure that the solvent was poor for all the blocks.

## Results and discussion

Clearly, the confined self-assembly of ABC triblock copolymers is largely dominated by a series of controlling parameters, including polymer–polymer interactions, polymer–solvent interactions and the length ratios of A, B and C blocks. The influence of these parameters on the self-assembled nanostructure is considered in this study. Fig. 1 shows a series of aggregates from the symmetrical  $A_7B_7C_7$  triblock copolymers at different polymer–solvent interactions. When  $\epsilon_{AS} < \epsilon_{BS} < \epsilon_{CS}$  ( $\epsilon_{AS} = 1.0$ ,  $\epsilon_{BS} = 2.0$  and  $\epsilon_{CS} = 3.0$ , Fig. 1a),  $A_7B_7C_7$  triblock copolymers aggregate into a tapered nanoparticle with the weak hydrophobic A lamellae covered at bottom and top of the nanoparticle. This tapered nanoparticle is similar to the bud-like nanoparticle in experiments.<sup>17</sup> When A, B, and C blocks possess the same hydrophobicity (*i.e.*  $\epsilon_{AS} = \epsilon_{BS} = \epsilon_{CS} = 3.0$ ), an ellipsoidal pupa-like nanoparticle is formed by  $A_7B_7C_7$  triblock copolymers, as shown in Fig. 1b. When the hydrophobicity of A, B and C blocks decreases progressively, a reversed bud-like nanoparticle is observed, as shown in Fig. 1c. This morphological transition from a bud-like particle to a pupa-like particle, and then back to the bud-like particle agrees well with the experimental observation.<sup>17</sup> The simulation results indicate that the terminal blocks (A or C block) with weaker hydrophobicity are always at the bottom and top of the bud-like particle to reduce the energy of the system.<sup>39</sup>

Compared to the symmetrical block copolymers, more unique nanostructures may be obtained from the self-assembly of asymmetrical block copolymers due to their asymmetric chain architectures. In the current study, three types of asymmetrical ABC triblock copolymers, *i.e.*  $A_4B_{13}C_4$ ,  $A_{13}B_4C_4$  and  $A_8B_5C_8$ , are considered in the following section. In these asymmetric block copolymers,  $A_4B_{13}C_4$  possesses a relatively long middle block,  $A_{13}B_4C_4$  contains a relatively long terminal block, whereas  $A_8B_5C_8$  has two long terminal blocks and a short middle block. Fig. 2 shows a series of typical aggregates formed by  $A_4B_{13}C_4$  triblock copolymers as a function of polymer–solvent interactions (*i.e.*  $\epsilon_{PS}$ , we set  $\epsilon_{PS} = \epsilon_{AS} = \epsilon_{BS} = \epsilon_{CS}$ ). When  $\epsilon_{PS} \leq 5.0$ , ABC triblock copolymers tend to aggregate into a novel nanostructure with a striped-pattern on the surface of the nanoparticle. From the top images, it is observed that A and C

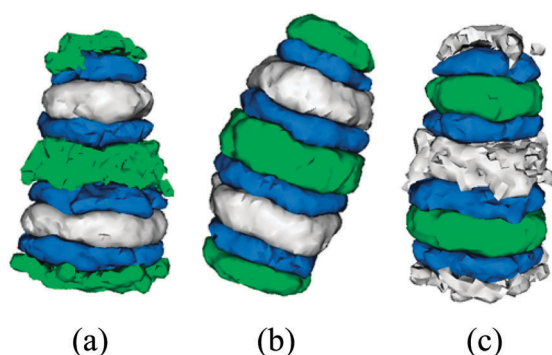


Fig. 1 Typical aggregates from symmetrical  $A_7B_7C_7$  triblock copolymers at different  $\epsilon_{AS}$ ,  $\epsilon_{BS}$ , and  $\epsilon_{CS}$ . (a)  $\epsilon_{AS} = 1.0$ ,  $\epsilon_{BS} = 2.0$  and  $\epsilon_{CS} = 3.0$ ; (b)  $\epsilon_{AS} = \epsilon_{BS} = \epsilon_{CS} = 3.0$ ; (c)  $\epsilon_{AS} = 3.0$ ,  $\epsilon_{BS} = 2.0$  and  $\epsilon_{CS} = 1.0$ .  $\epsilon_{AB} = \epsilon_{BC} = \epsilon_{AC} = 3.0$  for (a–c). ■ represents the A blocks; ■ represents the B blocks; ■ represents the C blocks.

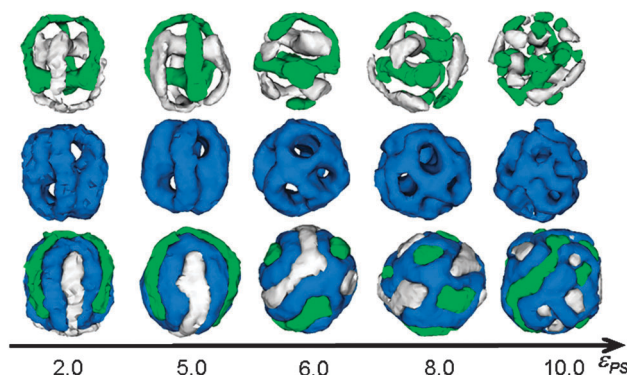
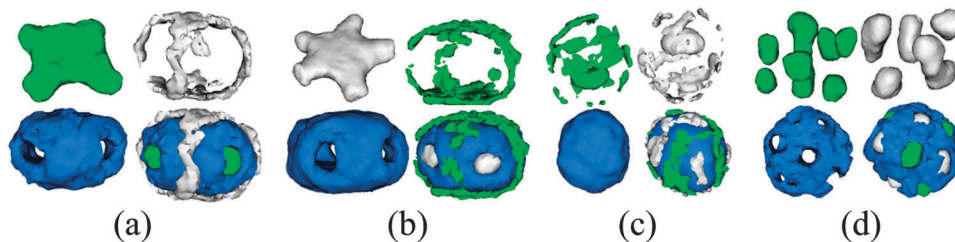


Fig. 2 A series of typical aggregates from asymmetrical  $A_4B_{13}C_4$  triblock copolymers as a function of  $\epsilon_{PS}$ .  $\epsilon_{PS} = \epsilon_{AS} = \epsilon_{BS} = \epsilon_{CS}$  and  $\epsilon_{AB} = \epsilon_{BC} = \epsilon_{AC} = 3.0$ . The color codes are the same as that in Fig. 1.

blocks tend to form the cage-like structure. More interestingly, the A-cage and the C-cage are intertwined with each other, as shown in Fig. 2. As  $\epsilon_{PS}$  is increased, A and C stripes start to break up into some short stripes ( $\epsilon_{PS} = 6.0$ ), and then into a larger number of small patches ( $\epsilon_{PS} = 8.0$  or  $\epsilon_{PS} = 10.0$ ). With the increase of the hydrophobicity,  $A_4B_{13}C_4$  triblock copolymers tend to aggregate into a more compact nanoparticle to reduce the contact between the hydrophobic blocks and the solvents. Because of the shrinking of nanoparticles, the short A and C blocks can no longer form long stripes, which can only form some small patches embedded in the porous B shell.

In Fig. 2, A, B and C blocks possess the same hydrophobicity, *i.e.*  $\epsilon_{AS} = \epsilon_{BS} = \epsilon_{CS}$ . Clearly, the hydrophobicity of each block also plays an important role in the self-assembly. The blocks with weaker hydrophobicity are more likely to distribute on the surface of the aggregated nanoparticle, whereas the blocks with stronger hydrophobicity tend to form the inner core to avoid the contact with the solvents. To examine the effect of hydrophobicity of each block on the self-assembled nanostructures, we present a series of aggregated morphologies of  $A_4B_{13}C_4$  triblock copolymers with different  $\epsilon_{AS}$ ,  $\epsilon_{BS}$  and  $\epsilon_{CS}$  in Fig. 3. When A blocks possess relatively higher hydrophobicity than the B and C blocks (*i.e.*  $\epsilon_{AS} = 4.0$  and  $\epsilon_{BS} = \epsilon_{CS} = 2.0$ , Fig. 3a), A blocks tend to aggregate into a polygonal core, whereas B and C blocks form a porous shell and cage, respectively. In contrast, C blocks are more likely to aggregate into a pentacle core, and B and A blocks form the porous shell and cage, respectively, when B and C blocks are more hydrophobic than the A blocks ( $\epsilon_{AS} = 2.0$  and  $\epsilon_{BS} = \epsilon_{CS} = 4.0$ , Fig. 3b). When the middle B blocks are more hydrophobic than the two terminal blocks, *i.e.* A and C blocks, ABC triblock copolymers self-assemble into nanoparticles with A and C stripes on the surface ( $\epsilon_{AS} = \epsilon_{CS} = 2.0$  and  $\epsilon_{BS} = 5.0$ , Fig. 3c). It is interesting to observe that A and C blocks form two hemispheres in the center of the nanoparticle, as shown in the top images of Fig. 3c. When the A and C blocks possess higher hydrophobicity than the middle B blocks ( $\epsilon_{AS} = \epsilon_{CS} = 5.0$  and  $\epsilon_{BS} = 2.0$ ), ABC triblock copolymers form a patch-like nanoparticle, as shown in Fig. 3d. This patch-like nanoparticle is composed of a large number of small A and C spheres and a porous B shell.





**Fig. 3** Typical aggregates from asymmetrical  $A_4B_{13}C_4$  triblock copolymers at different  $\epsilon_{AS}$ ,  $\epsilon_{BS}$  and  $\epsilon_{CS}$ . (a)  $\epsilon_{AS} = 4.0$ ,  $\epsilon_{BS} = \epsilon_{CS} = 2.0$ ; (b)  $\epsilon_{AS} = 2.0$ ,  $\epsilon_{BS} = \epsilon_{CS} = 4.0$ ; (c)  $\epsilon_{AS} = \epsilon_{CS} = 2.0$ ,  $\epsilon_{BS} = 5.0$ ; (d)  $\epsilon_{AS} = \epsilon_{CS} = 5.0$ ,  $\epsilon_{BS} = 2.0$ . The color codes are the same as that in Fig. 1.

The confined self-assembly of asymmetrical  $A_{13}B_4C_4$  triblock copolymers is also examined. Fig. 4 presents the typical aggregates formed by  $A_{13}B_4C_4$  triblock copolymers as a function of  $\epsilon_{PS}$  ( $\epsilon_{PS} = \epsilon_{AS} = \epsilon_{BS} = \epsilon_{CS}$ ). When  $\epsilon_{PS} = 2.0$ ,  $A_{13}B_4C_4$  triblock copolymers aggregate into a pyramid-like nanoparticle, as shown in Fig. 4. It is interesting to note that B and C blocks form four Janus lamellae adhered onto the four surfaces of the pyramid-like nanoparticle. As  $\epsilon_{PS}$  is increased to 3.0, A blocks are more likely to form a dumbbell-like core, while B and C blocks assemble into two Janus lamellae and a Janus ring surrounding the A-core. As  $\epsilon_{PS}$  is further increased, isolated Janus B-C lamellae tend to coalesce into one Janus stripe, as shown in images in Fig. 4 ( $\epsilon_{PS} = 6.0$  and  $\epsilon_{PS} = 8.0$ ). More interestingly, B and C blocks form a helical Janus stripe around the A-core when  $\epsilon_{PS}$  is 8.0. As the hydrophobic degree is increased from 2.0 to 8.0, the shape of the self-assembled nanoparticle transitions from a tetrahedron ( $\epsilon_{PS} = 2.0$ ) to an ellipsoid ( $\epsilon_{PS} = 3.0$ ), and then to a sphere ( $\epsilon_{PS} = 6.0$  and  $\epsilon_{PS} = 8.0$ ). Clearly, this transition can effectively reduce the surface area of the nanoparticle, which can decrease the contacts between the hydrophobic blocks and the poor solvents.

In Fig. 5, we present a series of typical aggregates from asymmetrical  $A_{13}B_4C_4$  triblock copolymers when A, B and C blocks possess different hydrophobic properties. When the hydrophobic properties of A, B and C blocks are decreased in turn ( $\epsilon_{AS} = 4.0$ ,  $\epsilon_{BS} = 3.0$  and  $\epsilon_{CS} = 2.0$ ), ABC triblock copolymers aggregate into a novel cubic nanoparticle (Fig. 5a). It can be seen that the highly hydrophobic A blocks form a cube-shape

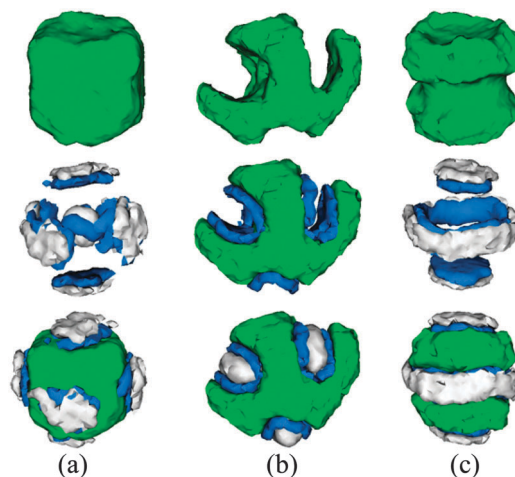


**Fig. 5** Typical aggregates from asymmetrical  $A_{13}B_4C_4$  triblock copolymers at different  $\epsilon_{AS}$ ,  $\epsilon_{BS}$  and  $\epsilon_{CS}$ . (a)  $\epsilon_{AS} = 4.0$ ,  $\epsilon_{BS} = 3.0$ ,  $\epsilon_{CS} = 2.0$ ; (b)  $\epsilon_{AS} = \epsilon_{BS} = 2.0$ ,  $\epsilon_{CS} = 4.0$ ; (c)  $\epsilon_{AS} = \epsilon_{CS} = 2.0$ ,  $\epsilon_{BS} = 6.0$ . The color codes are the same as that in Fig. 1.

core, whereas the weak hydrophobic B and C blocks form six Janus lamellae adhered onto the surfaces of the A-cube. Moreover, it is observed that parts of B and C blocks co-assemble into an inner core embedded inside the A-cube. When C blocks possess higher hydrophobicity than A and B blocks ( $\epsilon_{AS} = \epsilon_{BS} = 2.0$ ,  $\epsilon_{CS} = 4.0$ ), A blocks form a W-shape shell, whereas B and C blocks form the curved lamellae and short rods, respectively, filled in the cracks of the W-shape A shell (Fig. 5b). In this nanostructure, the highly hydrophobic C blocks are embedded, which can minimize their exposure to a poor solvent environment. When the middle B block has higher hydrophobicity than the A and C blocks ( $\epsilon_{AS} = \epsilon_{CS} = 2.0$ ,  $\epsilon_{BS} = 6.0$ ), A blocks form a dumbbell-shape core, B and C blocks form the Janus lamellae and ring surrounding the dumbbell-shape A-core (Fig. 5c), which is similar to the self-assembled nanostructure shown in Fig. 4 (images taken at  $\epsilon_{AS} = \epsilon_{BS} = \epsilon_{CS} = 3.0$ ).

For the asymmetrical  $A_8B_5C_8$  triblock copolymer, it contains two relatively long end blocks (A and C blocks) and a relatively short middle B block, which has different chain architecture from the asymmetrical  $A_4B_{13}C_4$  and  $A_{13}B_4C_4$  copolymers. A series of resulting aggregates at different polymer-solvent interactions ( $\epsilon_{PS}$ ) are presented in Fig. 6. When  $\epsilon_{PS} = 3.0$  or  $\epsilon_{PS} = 6.0$ , a classic pupa-like particle containing the A-C alternating structure is observed. As  $\epsilon_{PS}$  is increased ( $\epsilon_{PS} = 7.0$  or  $\epsilon_{PS} = 8.0$ ),

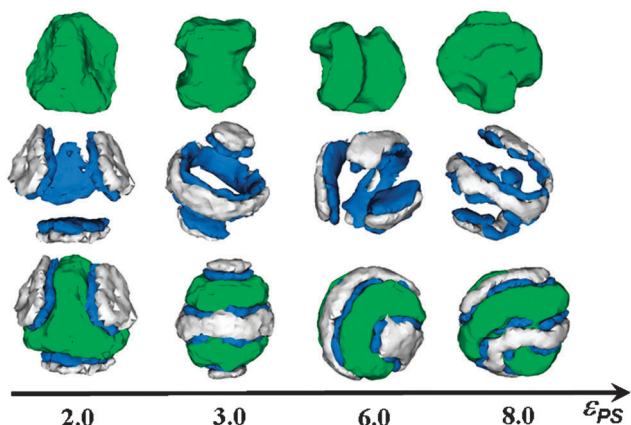


**Fig. 4** A series of typical aggregates from asymmetrical  $A_{13}B_4C_4$  triblock copolymers as a function of  $\epsilon_{PS}$ .  $\epsilon_{PS} = \epsilon_{AS} = \epsilon_{BS} = \epsilon_{CS}$  and  $\epsilon_{AB} = \epsilon_{BC} = \epsilon_{AC} = 3.0$ . The color codes are the same as that in Fig. 1.

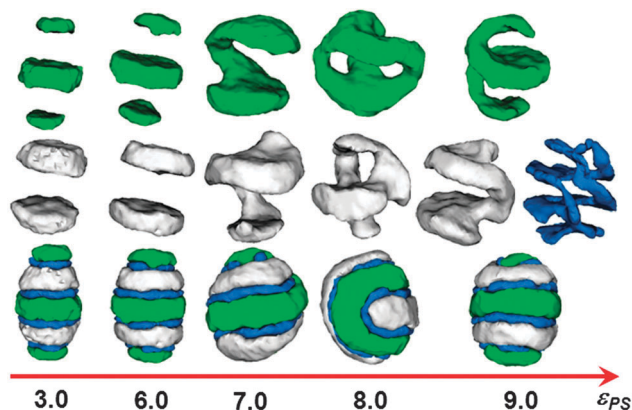


Fig. 6 A series of typical aggregates from asymmetrical  $A_8B_5C_8$  triblock copolymers as a function of  $\epsilon_{PS}$ .  $\epsilon_{PS} = \epsilon_{AS} = \epsilon_{BS} = \epsilon_{CS}$  and  $\epsilon_{AB} = \epsilon_{BC} = \epsilon_{AC} = 3.0$ . The color codes are the same as that in Fig. 1.

parallel A, B and C lamellae transition into the distorted lamellae. Moreover, it is interesting to note that A, B and C blocks are more likely to form the helical structures when  $\epsilon_{PS}$  is increased to 9.0, as shown in Fig. 6. From the images at  $\epsilon_{PS} = 9.0$ , it is observed that the two end blocks, *i.e.* A and C blocks, form the helical structures, whereas the middle B blocks aggregate into a double-helix structure.

To date, very limited information has been available for the formation pathway of the micelles because of the difficult in tracing the morphological transition by the off-line technique such as transmission electron microscopy (TEM). Monte Carlo simulation has been proved to be an effective method to explore

the kinematic pathway for the self-assembled micelles.<sup>18,28,40–42</sup> In the following section, the formation mechanisms of some novel self-assembled nanoparticles are examined. Fig. 7 presents the variations of the contact numbers ( $N_{AS}$ ,  $N_{BS}$  and  $N_{AC}$ ) with time for the  $A_4B_{13}C_4$  triblock copolymers at  $\epsilon_{AS} = \epsilon_{BS} = \epsilon_{CS} = 2.0$ . At this interaction setting,  $A_4B_{13}C_4$  triblock copolymers aggregate into a striped-pattern nanoparticle with an intertwined A-cage and C-cage, as shown in Fig. 2. To visualize the formation pathway of this novel nanostructure, a series of snapshots at different times are also inserted in Fig. 7.  $N_{AS}$  and  $N_{BS}$  are the contact numbers between monomers (A or B) and solvents, indicating the micellization of block copolymers.  $N_{AC}$  is the contact number between the immiscible A and C monomers, which can be used to monitor the microphase separation between the A and C blocks. As can be seen from the  $N_{AS}$ - $t$  and  $N_{BS}$ - $t$  curves,  $N_{AS}$  and  $N_{BS}$  show a steady decline with time until  $t = 380$  (micellization), and then remain mostly unchanged as time further increases (micellization completed).  $N_{AC}$  increases considerably with time and then reaches its peak at  $t = 170$ . Thereafter,  $N_{AC}$  slightly decreases with time up to  $t = 380$ , and then remains unchanged as time further increases. Clearly, the contact between A and C will increase when the randomly dispersed ABC triblock copolymers aggregate into a polymer droplet under soft confinement. Therefore, the initial increase of  $N_{AC}$  with time is attributed to the aggregation of  $A_4B_{13}C_4$  triblock copolymers, whereas the subsequent decrease of  $N_{AC}$  is caused by the microphase separation between the immiscible A and C blocks. The formation pathway of the resulting striped-pattern is visualized by a series inserted snapshots of the block copolymers. It is observed that the  $A_4B_{13}C_4$  triblock copolymers

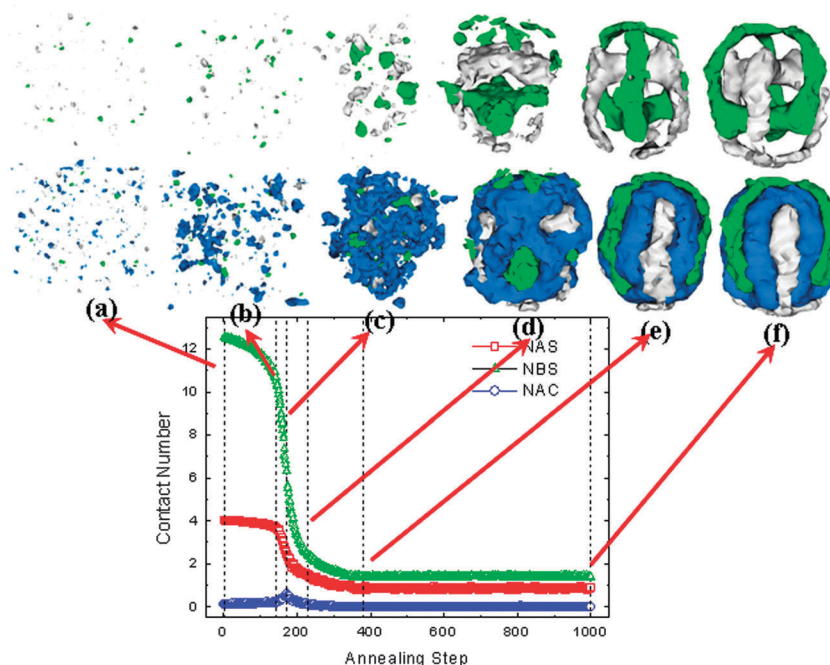
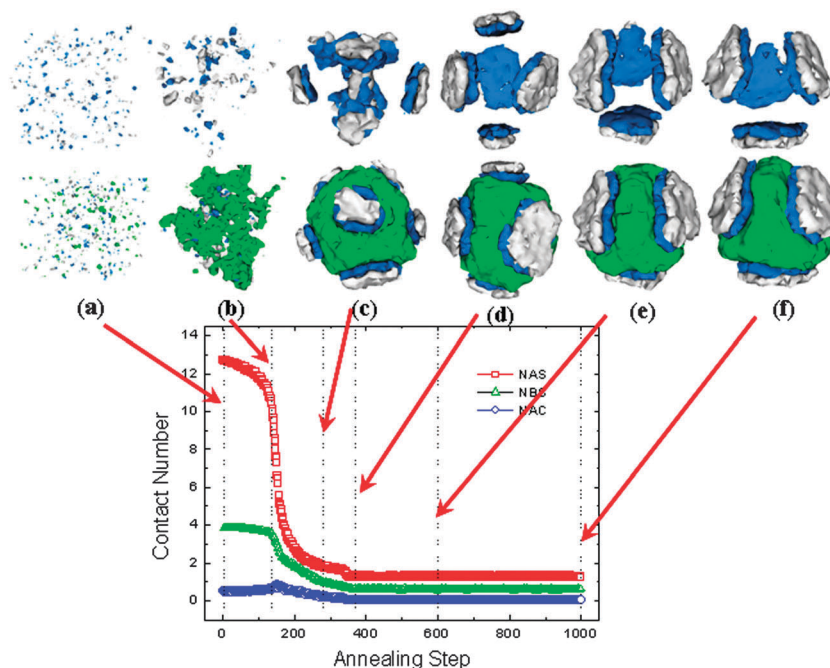


Fig. 7 Variations of the numbers of contacts,  $N_{AS}$ ,  $N_{BS}$  and  $N_{AC}$ , with time for asymmetrical  $A_4B_{13}C_4$  triblock copolymers at  $\epsilon_{AS} = \epsilon_{BS} = \epsilon_{CS} = 2.0$ . Typical snapshots at different times are also inserted in this diagram to show the formation pathway of the striped-pattern nanoparticle with intertwined A-cages and C-cages: (a)  $t = 1$ ; (b)  $t = 141$ ; (c)  $t = 170$ ; (d)  $t = 230$ ; (e)  $t = 380$ ; (f)  $t = 1000$ . The color codes for the snapshots are the same as that in Fig. 1.

gradually aggregate together (Fig. 7a and b) at first, and then form a loose aggregate at  $t = 170$  (Fig. 7c), when the quality of solvent gradually transitions from good to poor. Thereafter, the microphase separation between A, B and C blocks occurs, resulting in the formation of a more compact nanoparticle with the striped-pattern (Fig. 7d and e,  $380 \geq t \geq 230$ ). In a

striped-pattern nanoparticle, A and C blocks form two cages intertwined with each other. This striped-pattern structure remains almost unchanged as the annealing step further increases (Fig. 7f,  $t = 1000$ ).

For the unique pyramid-like nanoparticle, its formation mechanism is also examined by the variations of contact numbers



**Fig. 8** Variations of the numbers of contacts,  $N_{AS}$ ,  $N_{BS}$  and  $N_{AC}$ , with time for asymmetrical  $A_{13}B_4C_4$  triblock copolymers at  $\epsilon_{AS} = \epsilon_{BS} = \epsilon_{CS} = 2.0$ . Typical snapshots at different times are also inserted in this diagram to show the formation pathway of the nanoparticle with a pyramid-like A-core and four Janus BC lamellae adhered onto the four surfaces of the pyramid-like A-core: (a)  $t = 1$ ; (b)  $t = 137$ ; (c)  $t = 280$ ; (d)  $t = 370$ ; (e)  $t = 600$ ; (f)  $t = 1000$ . The color codes for the snapshots are the same as that in Fig. 1.

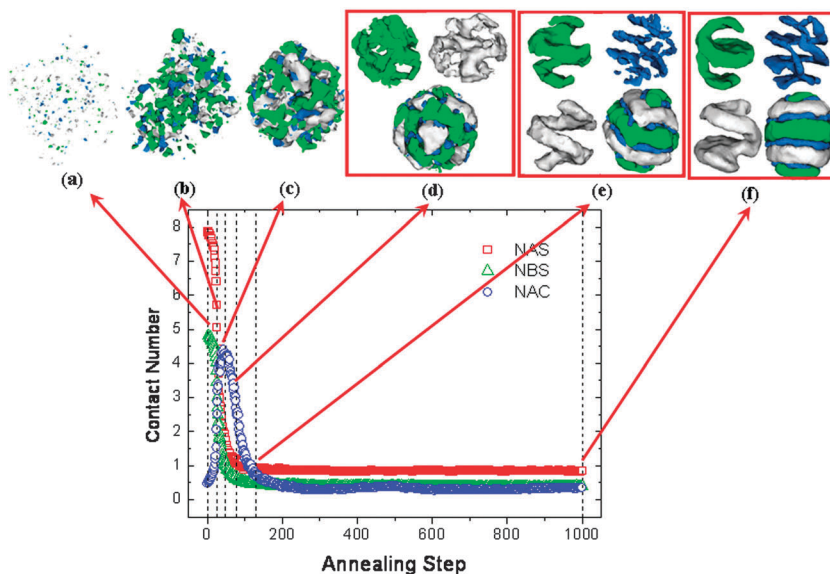


**Fig. 9** Variations of the numbers of contacts,  $N_{AS}$ ,  $N_{BS}$  and  $N_{AC}$ , with time for asymmetrical  $A_8B_5C_8$  triblock copolymers at  $\epsilon_{AS} = \epsilon_{BS} = \epsilon_{CS} = 9.0$ . Typical snapshots at different times are also inserted in this diagram to show the formation pathway of the nanoparticle containing helical A, B and C structures: (a)  $t = 1$ ; (b)  $t = 26$ ; (c)  $t = 47$ ; (d)  $t = 78$ ; (e)  $t = 130$ ; (f)  $t = 1000$ . The color codes for the snapshots are the same as that in Fig. 1.



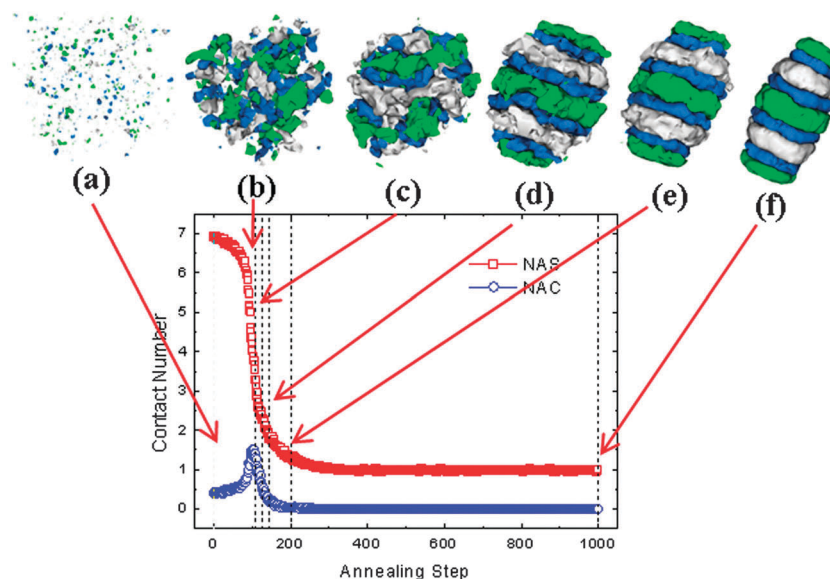


**Fig. 10** Variations of the numbers of contacts,  $N_{AS}$ ,  $N_{BS}$  and  $N_{AC}$ , with time for symmetrical  $A_7B_7C_7$  triblock copolymers at  $\epsilon_{AS} = \epsilon_{BS} = \epsilon_{CS} = 3.0$ . Typical snapshots at different times are also inserted in this diagram to show the formation pathway of ellipsoidal pupa-like nanoparticles: (a)  $t = 1$ ; (b)  $t = 107$ ; (c)  $t = 125$ ; (d)  $t = 142$ ; (e)  $t = 200$ ; (f)  $t = 1000$ . The color codes for the snapshots are the same as that in Fig. 1.

and a series of snapshots at different times, as shown in Fig. 8. From the snapshots in Fig. 8,  $A_{13}B_4C_4$  triblock copolymers firstly form a loose aggregate (Fig. 8a and b), and then A blocks form a polyhedral core, whereas B and C blocks aggregate into some small Janus lamellae on the surface of the A-core, as shown in Fig. 8c. As time further increases, the polyhedral A-core

transitions into a tetrahedral shape, whereas small Janus B-C lamellae coalesce into four big Janus lamellae adhered onto the four surfaces of the tetrahedron, as shown in Fig. 8c-f. The variations of the contact numbers with time are also presented in Fig. 8. Similarly,  $N_{AC}$  increases to the maximum value when  $A_{13}B_4C_4$  triblock copolymers form a loose aggregate ( $t = 141$ , Fig. 8b), and then declines because of the microphase separation between A, B and C blocks.  $N_{AS}$  and  $N_{BS}$  show a steady decline with time during the micellization ( $t \leq 280$ ), and then remain mostly unchanged as time further increases ( $t > 280$ ). The formation mechanisms of the nanoparticles containing helical A, B and C structures and the ellipsoidal pupa-like nanoparticles are also investigated, as shown in Fig. 9 and 10. Similarly, ABC triblock copolymers firstly aggregate into a loose aggregate, and then the microphase separation between the immiscible A, B and C occurs, resulting in the formation of the final nanostructures.

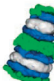




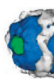










To better understand the inner relationship between the self-assembled nanostructures with the block copolymer architectures, the incompatibilities between different block types, and solvent properties, we summarized all the predicted nanostructures in Table 1.

## Conclusions

Using the Monte Carlo technique, the self-assembly of ABC triblock copolymers under 3D soft-confinement is systematically investigated by varying a series of control parameters, such as the symmetry of the ABC triblock copolymers, incompatibility between the different types of the blocks, and the solvent quality for the solvophobic blocks. A rich variety of novel nanostructures are obtained *via* the Monte Carlo simulations. The relationship between the self-assembled nanostructures and the control parameters, such as the symmetry of the block copolymer,

**Table 1** Summarization of the predicted nanostructures as a function of block copolymer architectures, the incompatibilities between different block types, and solvent properties

ABC triblock copolymer Self-assembled nanostructures

$A_7B_7C_7$	 $\epsilon_{AS}=1.0$ $\epsilon_{BS}=2.0$ $\epsilon_{CS}=3.0$	 $\epsilon_{AS}=3.0$ $\epsilon_{BS}=3.0$ $\epsilon_{CS}=3.0$	 $\epsilon_{AS}=3.0$ $\epsilon_{BS}=2.0$ $\epsilon_{CS}=1.0$		
$A_4B_{13}C_4$	 $\epsilon_{AS}=2.0$ $\epsilon_{BS}=2.0$ $\epsilon_{CS}=2.0$	 $\epsilon_{AS}=10.0$ $\epsilon_{BS}=10.0$ $\epsilon_{CS}=10.0$	 $\epsilon_{AS}=4.0$ $\epsilon_{BS}=2.0$ $\epsilon_{CS}=2.0$	 $\epsilon_{AS}=5.0$ $\epsilon_{BS}=2.0$ $\epsilon_{CS}=5.0$	
$A_{13}B_4C_4$	 $\epsilon_{AS}=2.0$ $\epsilon_{BS}=2.0$ $\epsilon_{CS}=2.0$	 $\epsilon_{AS}=3.0$ $\epsilon_{BS}=3.0$ $\epsilon_{CS}=3.0$	 $\epsilon_{AS}=8.0$ $\epsilon_{BS}=8.0$ $\epsilon_{CS}=8.0$	 $\epsilon_{AS}=4.0$ $\epsilon_{BS}=3.0$ $\epsilon_{CS}=2.0$	 $\epsilon_{AS}=2.0$ $\epsilon_{BS}=2.0$ $\epsilon_{CS}=4.0$
$A_8B_5C_8$	 $\epsilon_{AS}=3.0$ $\epsilon_{BS}=3.0$ $\epsilon_{CS}=3.0$	 $\epsilon_{AS}=7.0$ $\epsilon_{BS}=7.0$ $\epsilon_{CS}=7.0$	 $\epsilon_{AS}=8.0$ $\epsilon_{BS}=8.0$ $\epsilon_{CS}=8.0$	 $\epsilon_{AS}=9.0$ $\epsilon_{BS}=9.0$ $\epsilon_{CS}=9.0$	



incompatibilities between different block types, and solvent properties, are revealed, which helps to design the novel nanostructures in experiment. Moreover, the formation pathways of some typical self-assembled nanostructures imply that the ABC triblock copolymers tend to form a loose aggregate at first, and then the microphase separation between A, B and C blocks occurs due to the immiscibility, resulting in the formation of the unique nanostructures.

## Acknowledgements

This work was financially supported by the National Natural Science Foundation of China for General Program (51373172), Major Program (51433009), and the Open Project of State Key Laboratory of Supramolecular Structure and Materials (sklssm2015030).

## References

- X. H. He, M. Song, H. J. Liang and C. Y. Pan, *J. Chem. Phys.*, 2001, **114**, 10510–10513.
- A. C. Arsenault, D. A. Rider, N. Tetreault, J. I. L. Chen, N. Coombs, G. A. Ozin and I. Manners, *J. Am. Chem. Soc.*, 2005, **127**, 9954–9955.
- B. Yu, B. Li, Q. Jin, D. Ding and A.-C. Shi, *Macromolecules*, 2007, **40**, 9133–9142.
- Y. Zhu and W. Jiang, *Macromolecules*, 2007, **40**, 2872–2881.
- P. Chen, H. Liang and A.-C. Shi, *Macromolecules*, 2008, **41**, 8938–8943.
- T. Tanaka, N. Saito and M. Okubo, *Macromolecules*, 2009, **42**, 7423–7429.
- P. Chi, Z. Wang, B. Li and A.-C. Shi, *Langmuir*, 2011, **27**, 11683–11689.
- N. Yan, Y. Sheng, H. Liu, Y. Zhu and W. Jiang, *Langmuir*, 2015, **31**, 1660–1669.
- H. H. Pham, I. Gourevich, J. K. Oh, J. E. N. Jonkman and E. Kumacheva, *Adv. Mater.*, 2004, **16**, 516–520.
- J. Y. Cheng, C. A. Ross, H. I. Smith and E. L. Thomas, *Adv. Mater.*, 2006, **18**, 2505–2521.
- R. Deng, F. Liang, X. Qu, Q. Wang, J. Zhu and Z. Yang, *Macromolecules*, 2015, **48**, 750–755.
- D. Klinger, C. X. Wang, L. A. Connal, D. J. Audus, S. G. Jang, S. Kraemer, K. L. Killops, G. H. Fredrickson, E. J. Kramer and C. J. Hawker, *Angew. Chem., Int. Ed.*, 2014, **53**, 7018–7022.
- S.-J. Jeon, G.-R. Yi and S.-M. Yang, *Adv. Mater.*, 2008, **20**, 4103–4108.
- R. Deng, S. Liu, J. Li, Y. Liao, J. Tao and J. Zhu, *Adv. Mater.*, 2012, **24**, 1889–1893.
- R. Deng, F. Liang, W. Li, S. Liu, R. Liang, M. Cai, Z. Yang and J. Zhu, *Small*, 2013, **9**, 4099–4103.
- J. Zhu and R. C. Hayward, *Macromolecules*, 2008, **41**, 7794–7797.
- J. Xu, K. Wang, J. Li, H. Zhou, X. Xie and J. Zhu, *Macromolecules*, 2015, **48**, 2628–2636.
- Y. Sheng, J. An and Y. Zhu, *Chem. Phys.*, 2015, **452**, 46–52.
- B. Yu, J. Deng, B. Li and A.-C. Shi, *Soft Matter*, 2014, **10**, 6831–6843.
- D. J. Pochan, Z. Y. Chen, H. G. Cui, K. Hales, K. Qi and K. L. Wooley, *Science*, 2004, **306**, 94–97.
- J. T. Zhu and W. Jiang, *Macromolecules*, 2005, **38**, 9315–9323.
- H. Cui, Z. Chen, S. Zhong, K. L. Wooley and D. J. Pochan, *Science*, 2007, **317**, 647–650.
- S. Zhong, H. Cui, Z. Chen, K. L. Wooley and D. J. Pochan, *Soft Matter*, 2008, **4**, 90–93.
- J. Dupont, G. Liu, K.-i. Niihara, R. Kimoto and H. Jinnai, *Angew. Chem., Int. Ed.*, 2009, **48**, 6144–6147.
- W. Kong, B. Li, Q. Jin, D. Ding and A.-C. Shi, *J. Am. Chem. Soc.*, 2009, **131**, 8503–8512.
- J. Dupont and G. Liu, *Soft Matter*, 2010, **6**, 3654–3661.
- Y. Zhu, X. Yang, W. Kong, Y. Sheng and N. Yan, *Soft Matter*, 2012, **8**, 11156–11162.
- Y. Zhu, H. Yu, Y. Wang, J. Cui, W. Kong and W. Jiang, *Soft Matter*, 2012, **8**, 4695–4707.
- W. Kong, W. Jiang, Y. Zhu and B. Li, *Langmuir*, 2012, **28**, 11714–11724.
- Y. Sheng, N. Yan, J. An and Y. Zhu, *Chem. Phys.*, 2014, **441**, 47–52.
- Z. Li, M. A. Hillmyer and T. P. Lodge, *Langmuir*, 2006, **22**, 9409–9417.
- S. Li, Y. Jiang and J. Z. Y. Chen, *Soft Matter*, 2013, **9**, 4843–4854.
- R. G. Larson, L. E. Scriven and H. T. Davis, *J. Chem. Phys.*, 1985, **83**, 2411–2420.
- R. G. Larson, *J. Chem. Phys.*, 1988, **89**, 1642–1650.
- R. G. Larson, *J. Chem. Phys.*, 1989, **91**, 2479–2488.
- K. R. Haire, T. J. Carver and A. H. Windle, *Comput. Theor. Polym. Sci.*, 2001, **11**, 17–28.
- S. C. Ji and J. D. Ding, *Langmuir*, 2006, **22**, 553–559.
- N. Metropolis, A. W. Rosenbluth, M. N. Rosenbluth, A. H. Teller and E. Teller, *J. Chem. Phys.*, 1953, **21**, 1087–1092.
- R. Deng, F. Liang, W. Li, Z. Yang and J. Zhu, *Macromolecules*, 2013, **46**, 7012–7017.
- Y. Han, H. Yu, H. Du and W. Jiang, *J. Am. Chem. Soc.*, 2010, **132**, 1144–1150.
- Y. Sheng, X. Yang, N. Yan and Y. Zhu, *Soft Matter*, 2013, **9**, 6254–6262.
- J. Cui and W. Jiang, *Langmuir*, 2010, **26**, 13672–13676.